Role of Zinc in MSW Fly Ash during Formation of Chlorinated Aromatics

ARTICLE *in* ENVIRONMENTAL SCIENCE & TECHNOLOGY · AUGUST 2011

Impact Factor: 5.33 · DOI: 10.1021/es201810u · Source: PubMed

3 AUTHORS, INCLUDING:

Takashi Fujimori
Kyoto University
45 PUBLICATIONS **169** CITATIONS
SEE PROFILE

Masaki Takaoka
Kyoto University
161 PUBLICATIONS **1,046** CITATIONS
SEE PROFILE

Environmental Science & Technology

ARTICLE

pubs.acs.org/est

Role of Zinc in MSW Fly Ash during Formation of Chlorinated Aromatics

Takashi Fujimori,*[,†,‡] Yuta Tanino,[†] and Masaki Takaoka[†]

[†]Department of Environmental Engineering, Graduate School of Engineering, Kyoto University, Katsura, Nisikyo-ku, 615-8540, Kyoto, Japan

[‡]Center for Material Cycles and Waste Management Research, National Institute for Environmental Studies (NIES), 16-2 Onogawa, Tsukuba, 305-8506, Ibaraki, Japan

Supporting Information

ABSTRACT: In this study, we determined the thermochemical role of zinc in municipal solid waste (MSW) fly ash. Zinc's role depended on its chemical form and the presence of other metal catalysts. When only zinc was present or it dominated other metal elements, chlorinated aromatic compound (aromatic-Cl) formation was promoted by zinc chloride but blocked by zinc oxide. When only zinc was present, such as in zinc metallurgical plants, some aromatic-Cls were generated and contaminated the environment. When zinc coexisted with other metal promoters in a thermal postcombustion solid phase, such as MSW incineration, Fourier-transform Zn K-edge extended X-ray absorption fine structure (EXAFS) analysis showed that the chemical forms of zinc were primarily chloride and/or oxide, and zinc chloride ($ZnCl_2$) was thermally stable in the solid phase. Thus, we used $ZnCl_2$ in coexistence experiments as a promoter to generate aromatic-Cls. Zinc chloride acted as a coexistent inhibitor of metal catalysis and precursor dimerization to generate aromatic-Cls. There were two coexistent inhibition mechanisms. First, a low-temperature transition of chlorine to the gas phase (low-Cl(g)) occurred with metal catalysts such as $CuCl_2$ and $FeCl_3$, confirmed by Cl K-edge near-edge X-ray absorption fine structure (NEXAFS) analysis. Second, X-ray photoelectron spectroscopy (XPS) analysis of the surface or near-surface concentration of $ZnCl_2$ indicated weak reactivity between the catalysts and the carbon matrix.

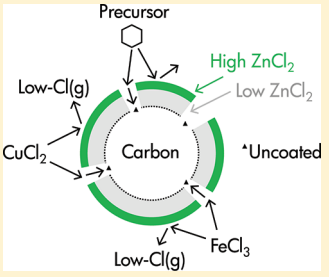

INTRODUCTION

Zinc is a major heavy metal produced anthropogenically in solid-phase compounds such as municipal solid waste (MSW) fly ash.[1−3] Researchers have reported that the zinc content in fly ash correlated positively with the concentrations of toxic chlorinated aromatic compounds (aromatic-Cls), such as polychlorinated dibenzo-p-dioxins (PCDDs),[4,5] furans (PCDFs),[5] biphenyls (PCBs),[6] and benzenes (CBzs).[6] Zinc metallurgical plants also emit PCDDs/Fs,[7,8] PCBs,[7,8] hexachlorobenzene,[8] and polychlorinated naphthalenes.[9] During postcombustion, zinc was thought to be generated as zinc chloride ($ZnCl_2$) or an oxide-like compound.[2,10−14] Zinc oxide (ZnO) and $ZnCl_2$ showed weak thermal catalytic activity in aromatic-Cl formation via particulate carbon[15−17] or precursors.[18] However, we cannot conclude that Zn compounds promoted aromatic-Cl formation because real systems are more complex than such models. In fact, Hinton and Lane reported data that refuted such a conclusion.[19] They studied the catalytic behavior of zinc using zinc compounds added to real fly ash. When zinc nitrate was added, higher concentrations of PCDDs were generated. However, PCDD content decreased with the addition of both zinc nitrate and copper nitrate. Their results suggested that zinc nitrate acted as an inhibitor when zinc coexisted with stronger metal promoters in real fly ash. The thermal behavior of solid-phase zinc as it relates to aromatic-Cl formation is still not fully understood. There has been no reported study on the thermochemical interaction between zinc and strong metal chlorides, such as $CuCl_2$ and $FeCl_3$, to promote aromatic-Cl formation.[16]

To determine whether zinc acts as a promoter, we performed systematic quantitative and X-ray spectroscopic experiments under coexistent conditions with $ZnCl_2$ at the temperature of aromatic-Cl formation. Real fly ashes (RFAs) at municipal solid waste incinerators (MSWIs) were used to determine the major chemical forms and thermal behavior of zinc. We prepared model fly ashes (MFAs) to understand the thermochemical interaction between zinc and metal chlorides ($CuCl_2$ and $FeCl_3$). Gas chromatography/mass spectrometry (GC/MS) experiments provided quantitative information on the aromatic-Cls. The thermochemical states of zinc and chlorine were analyzed by X-ray absorption fine structure (XAFS). Surface analysis by X-ray photoelectron spectroscopy (XPS) revealed characteristic zinc behavior in the solid phase. We discuss the coexistent-specific effects of zinc based on our results.

Received: May 27, 2011
Accepted: August 14, 2011
Revised: August 8, 2011
Published: August 15, 2011

MATERIALS AND METHODS

Sample Preparation. To study the behavior of zinc, we collected three types of RFAs (A, B, C) from the postcombustion zone bag filter or electrostatic precipitator of a MSWI in Japan and systematically prepared representative laboratory MFA samples: blank, Zn, Cu, Fe, CuZn, FeZn, [Zn], [Cu], [Fe], [CuZn], and [FeZn]. Sample compositions are shown in the Supporting Information (SI) and Table S1. The concentrations of heavy metal additives of inorganic chlorine and activated carbon (Shirasagi palm shell, 20−48 mesh; Takeda Pharmaceutical Co., Ltd., Osaka) in MFA were determined based on the compositions of the RFAs[1−3,6] and experimental restriction (see the SI). Concentrations of metals reflected those in real MSW fly ash because we wanted to examine the influence of trace metals on formation of aromatic-Cl compounds. Referring to the median values of eight RFAs in our previous study[6] and three RFAs (A, B, C) in this study, we prepared MFA samples. The organic compounds in activated carbon were removed by heating at 500 °C for 60 min under a stream of 100% nitrogen gas (100 mL/min). The MFA was ground in a mortar for about 10 min. MFA-blank was no addition of heavy metals. MFA-X series (X as metal chloride) indicated additive ratios of heavy metals of 0.2%Cu, 0.5%Fe, and 2.0%Zn and used for GC/MS, TOC, XPS, and Zn K-edge EXAFS experiments (Table S1). In contrast, all concentrations of heavy metals in MFA-[X] series were 5.0% metal. We analyzed Cl K-edge NEXAFS spectrum by applying MFA-[X] (SI and Table S1). We purchased SiO_2 (special grade), KCl (99.5%, special grade), $ZnCl_2$ (98.0%, special grade), $CuCl_2$ (98%), and $FeCl_3$ (97%) from Nacalai Tesque Inc., Japan and BN (special grade) from Wako Pure Chemical Industries, Ltd., Japan. Details of the sample preparation were reported in our previous publication.[16]

GC/MS and TOC Measurements. Samples (5 g) were placed in a quartz boat contained inside a quartz tube, which was then placed in a preheated electronic furnace at 300 °C[26,28] for 30 min under a flow of 10% oxygen/90% nitrogen,[28,29] delivered at 50 mL/min to simulate the postcombustion zone of a MSWI in Japan. After heating, the concentrations of PCBs and CBzs in the sample residue were analyzed by high-resolution GC/low-resolution MS (HP-6890/HP-5973). Pretreatment was performed to identify the chlorinated aromatic compounds according to Japanese Industrial Standards (JIS) K 0311 and 0312. For each heating experiment, analyses of PCBs and CBzs were duplicated (n = 2). Analytical details were reported in our previous publication.[16] Total organic carbon (TOC) was also measured as described previously.[21]

Surface Analysis by XPS. We performed XPS analysis (ESCA-3200, Shimadzu Corp.) to identify the chemical states near the surface (conditions of the MFAs are shown in Table S1) as a function of surface depth using argon ion etching. Measurement conditions included an X-ray source power (Mg Kα) of 8 kV and 30 mA, a pass energy of 75 eV, pressure $<10^{-6}$ Pa, beam voltage of 2 kV, beam current of 20 mA, step size of 0.1 eV, dwell time of 100 mS, and three sweeps. Argon ion etching was performed using an ion gun at the hot-cathode side. We used a sample rotation kit (SR-200) to grind the surface uniformly. Etching times were 0, 10, 60, and 180 s. Powder samples were applied to double-sided tape. We measured X-ray photoelectron spectra for C 1s, O 1s, Si 2p, Cl 2p, K 2p, Cu $2p_{3/2}$, Fe $2p_{3/2}$, Zn $2p_{3/2}$, and Zn $2p_{1/2}$. A charge correction was applied to the spectra using the C 1s energy (284.6 eV). The background was removed by the Shirley method.[27] Smoothing was accomplished using a quadric approximation, and calculations were repeated 20 times at nine-point intervals by the Savitsky-Golay method.[20] Atomic concentration was calculated using the peak area of an element and the relative sensitivity coefficient (C 1s = 1). Because silicon was thought to be an inactive element in the powder samples, relative ratios of atomic concentration were expressed as X/Si (where X is an element) to estimate elemental surface distributions. For example, Zn/Si indicates the atomic concentration of Zn over Si.

Zn K-Edge and Cl K-Edge X-ray Absorption Spectroscopy. The chemical states of zinc and chlorine were analyzed by XAFS. After the samples were ground in a mortar and an agate mortar for 10 min each, they were pressed into disks. We performed Zn K-edge extended XAFS (EXAFS) at BL01B1 in SPring-8 (Hyogo, Japan), with the sample disk heated in a T-type in situ cell under a flow of 10% oxygen/90% nitrogen delivered at 50 mL/min.[21−23] The temperature of the samples was increased from room temperature (rt) to 300 and 400 °C in a staircase pattern, as used in our previous experiments.[22] EXAFS spectra (energy range: 9440−10170 eV) were measured at rt, 300 °C, and 400 °C. After background removal and normalization, we obtained k^3-weighted, Fourier-transformed EXAFS spectra using the REX 2000 software (ver. 2.5.5; Rigaku, Japan). The peak positions of the Fourier-transformed spectra showed the elements bonded with zinc atoms, based on comparisons to reference spectra of zinc compounds (Zn, $ZnCl_2$, ZnO, $ZnCO_3$, ZnS, $ZnSO_4$, $ZnAl_2O_4$, $ZnFe_2O_4$, $Zn(OH)_2$, and $ZnPO_4$) and data reported by Struis et al.[12] Inversely Fourier-transformed spectra were analyzed by curve fitting with FEFF (ver. 8.10).

Cl K-edge near-edge XAFS (NEXAFS) analysis of powder samples was performed using BL-11B and BL-9A at the Photon Factory (Tsukuba, Japan). An in situ cell could not be used at Photon Factory because of the physical restrictions of the device. Powder samples were mounted on carbon tape, and NEXAFS spectra were collected by total fluorescence yield (TFY at 11B) or conversion electron yield (CEY at 9A) mode under vacuum or atmospheric pressure, respectively. Details of the procedure and Cl K-edge NEXAFS analysis were reported in our previous publications.[21,23,24]

RESULTS AND DISCUSSION

Chemical State of Zinc in Real Fly Ash. The nearest-neighbor elements of zinc in RFAs were chlorine or oxygen (Figure 1A), according to the peak positions of Zn K-edge Fourier-transformed EXAFS spectra. The shape of the Zn K-edge Fourier-transformed EXAFS spectrum of RFA-A was similar to that of the standard RFA (BCR176) measured by Struis et al.[12] A peak at ∼1.8 Å (= $R + \Delta R$) indicated Zn−Cl bonding, based on comparisons with the $ZnCl_2$ reference and previous study.[12] The primary chemical form of zinc in RFA-A was $ZnCl_2$. However, the EXAFS spectra of RFA-B and -C showed peaks at a shorter distance ($R + \Delta R$ = ∼1.5 Å; Figure 1A). From a previous study[12] and zinc oxide references, we concluded that the shorter peak distance was due to Zn−O bonding. Thus, the major chemical form of zinc in RFA-B and -C was thought to be ZnO. Analysis of Zn K-edge Fourier-transformed EXAFS indicated that the chemical state of zinc in the RFAs was primarily $ZnCl_2$ or ZnO. We previously reported that ZnO had zero or negative potential to promote the thermochemical formation of aromatic-Cls in the solid[16] and gas phases.[17] In the present study, we used $ZnCl_2$ as a promoter to generate aromatic-Cls.

Influence of Zinc on Aromatic-Cl Formation. Table 1 shows that the thermochemical formation of CBzs, D2-, P5-, H7-, and O8-chlorinated biphenyls at 300 °C were promoted to a greater extent by $ZnCl_2$ addition (MFA-Zn) than without metal addition (MFA-blank). Inorganic chloride (KCl) had a low potential to promote aromatic-Cl formation[24] but played a role as chlorine storage in case of coexistent with metal catalysts.[16,28] Because $CuCl_2$ and $FeCl_3$ addition greatly promoted CBzs and PCBs formation, compared with $ZnCl_2$ addition, the order of CBzs and PCBs formation was MFA-Cu > MFA-Fe > MFA-Zn > MFA-blank. Weight percents of zinc, copper, and iron in the MFAs were 2.0, 0.2, and 0.5%, respectively, and were based on representative studies on the chemical analysis of RFAs.[1−3,6] When $ZnCl_2$ was added under the conditions of our previous study (0.2% Zn at 300 °C), 24-ng/g ΣCBzs (D2-H6) and 2.8-ng/g ΣPCBs (D2-O8)[16] were produced. Under the conditions of the present study (2.0% Zn), 370-ng/g ΣCBzs and 14-ng/g ΣPCBs were produced. Thus, zinc content influenced aromatic-Cl formation. The concentration of CBzs showed a trend in the zinc-content effect: MFA-Zn (2.0% Zn), ΣCBzs =370 ng/g > MFA-Zn (0.2% Zn), 24 ng/g > MFA-blank (0% Zn), 21 ng/g. The concentration of PCBs did not conform to this tendency: MFA-blank (0% Zn), ΣPCBs = 18 ng/g > MFA-Zn (2.0% Zn), 14 ng/g > MFA-Zn (0.2% Zn), 2.8 ng/g. These different tendencies might be attributed to the difference of formation/destruction routes.

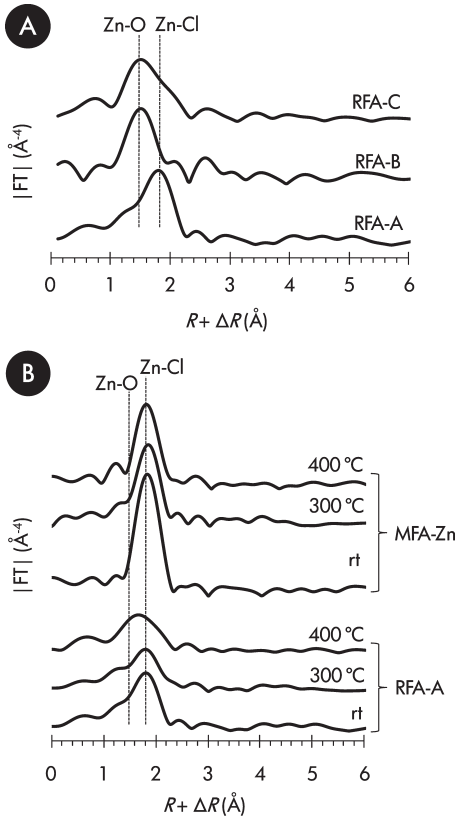

Figure 1. k^3 weighted Fourier-transformed Zn K-edge extended X-ray absorption fine structure (EXAFS). (A) Collected three type real fly ashes (RFA; A, B, and C) at room temperature (rt). (B) RFA-A and model fly ash admixed with zinc chloride (Zn) at room temperature (rt), 300 °C, and 400 °C.

We found that the coexistence of zinc with other trace metals ($CuCl_2$ and $FeCl_3$) was more effective for aromatic-Cl formation than zinc alone. Here, we defined inhibition effect in Table 1 as follows

$$\text{Inhibition of CuZn} = \left(1 - \frac{[\text{Ar}]_{\text{CuZn}}}{[\text{Ar}]_{\text{Cu}}}\right) \times 100, \text{ or}$$

$$\text{Inhibition of FeZn} = \left(1 - \frac{[\text{Ar}]_{\text{FeZn}}}{[\text{Ar}]_{\text{Fe}}}\right) \times 100 \quad (1)$$

where $[\text{Ar}]_X$ was concentration of aromatic-Cl (CBzs or PCBs) in the case of MFA-X. A negative value of inhibition effect ($[\text{Ar}]_{\text{YZn}} > [\text{Ar}]_{\text{Y}}$, Y = Cu or Fe) indicates that Zn was more effective in promoting the catalytic effect of metal Y. In contrast, a positive value of inhibition effect shows that Zn inhibited the catalytic effect of metal Y. When zinc chloride coexisted with cupric or ferric chloride (MFA-CuZn or FeZn), the concentrations of

Table 1. Concentrations of Chlorobenzenes (CBzs), Polychlorinated Biphenyls (PCBs), and Total Organic Carbon (TOC) after Heating Samples at 300 °C[a]

	blank (ng/g)	Zn (ng/g)	Cu (ng/g)	CuZn (ng/g)	inhibition of CuZn (%)	Fe (ng/g)	FeZn (ng/g)	inhibition of FeZn (%)
CBzs D2	18	100	230	1400	−530	78	810	−940
T3	0.86	62	670	620	6.8	460	610	−32
T4	0.33	75	5900	820	86	3000	1600	47
P5	0.30	94	5300	1300	75	4900	2300	54
H6	1.1	36	2500	2600	−4.4	3700	2800	24
ΣCBzs(D2-H6)	21	370	15000	6700	54	12000	8100	33
PCBs D2	0.94	2.7	4.4	6.1	−39	9.7	14	−45
T3	7.3	5.5	41	23	43	34	20	41
T4	7.5	4.2	54	16	71	36	20	45
P5	1.2	1.4	130	10	92	14	7.5	46
H6	1.0	0.25	180	13	93	32	11	64
H7	n.d.	0.34	320	12	96	36	12	65
O8	n.d.	0.02	430	16	96	49	16	68
ΣPCBs(D2-O8)	18	14	1200	96	92	210	100	52
TOC at 300 °C (%)	103	102	79	84		67	82	

[a] Inhibition of CuZn and that of FeZn were defined by eq 1 in text.

ΣCBzs (ΣPCBs) were inhibited to 54% (92%) or 33% (52%), compared with MFA-Cu or Fe, respectively (Table 1, Figure S1). T4- and P5-chlrorobenzenes in MFA-CuZn and FeZn showed a higher inhibitory effect, greater than 75 and 47%, respectively, than other congeners (Table 1, Figure S2A). Inhibitory effects greater than 92% and 64% were observed for PCBs from P5 to O8 in MFA-CuZn and from H6 to O8 in MFA-FeZn, respectively (Table 1, Figure S2B). A previous study reported that ΣPCDDs (T4−O8) were also inhibited by the coexistence of zinc nitrate with copper nitrate in fly ash compared with copper nitrate addition.[19] Thus, we concluded that the concentration inhibition of total aromatic-Cls and specific congeners at 300 °C was due to the coexistence of zinc with other strong promoters. In particular, the inhibition effect was greater for zinc chloride on cupric chloride than on ferric chloride with respect to total aromatic-Cl concentrations (Figure S1) and congener concentrations (Figure S2) of CBzs and PCBs. Additionally, Figure S1 shows visually that zinc chloride inhibited ΣPCBs (two aromatic rings) at higher rates than ΣCBzs (one ring) due to coexistence, indicating that the bridged structure of the aromatic ring did not form readily. An in-depth discussion of this unique phenomenon based on XPS and TOC data follows.

Thermochemical Behavior of Zinc and Chlorine. We studied the chemical state of zinc chloride at the temperature of aromatic-Cl formation to understand the thermochemical behavior of zinc. Under the same postcombustion conditions used for the quantitative heating experiments, the position of the primary peak of the in situ Zn K-Edge Fourier-transformed EXAFS spectrum of MFA-Zn did not change ($R + \Delta R =$ ~1.8 Å; Zn−Cl bonding) as the temperature increased from room temperature to 300 and 400 °C (Figure 1B). Thus, the bonding state of Zn−Cl was stable over this temperature range. Because the peak intensities at 300 and 400 °C were the same (coordination number of Cl, CN = 2.4−2.6) and weaker than that at room temperature (CN = 3.4), we suggest that a chlorine atom dissociated to some extent from $ZnCl_2$ up to 300 °C, and the surrounding Zn structure was stable from 300 to 400 °C. Aromatic-Cl formation at 300 °C (MFA-Zn in Table 1) was thought to be promoted by the dechlorination of zinc chloride. In-situ EXAFS measurements of RFA-A, in which zinc chloride was dominant, showed that Zn−Cl bonding was stable from room temperature to 300 °C, the peak intensity decreased slightly at 300 °C, and the peak shifted between the distances corresponding to Zn−Cl and Zn−O at 400 °C (Figure 1B). The thermochemical behavior of zinc chloride in RFA-A was the same as that in MFA-Zn from room temperature to 300 °C. However, the behavior in the two compounds differed at 400 °C, indicating that zinc was partially oxidized due to the presence of coexistent elements without zinc and the complex composition of real fly ash. We previously reported similar behavior (decreasing oxidation temperature) for cupric chloride.[25] Nonetheless, Zn K-edge EXAFS analysis confirmed that the thermochemical state of zinc chloride changed little and was thermally stable at ~300 °C, the temperature at which maximum aromatic-Cl formation occurs in real fly ashes.[26] These results were observed even when zinc coexisted with many elements in the solid phase, such as in RFA-A.

Although Zn−Cl bonding was stable in the complex solid phase, we observed unstable chlorine behavior with coexisting strong promoters, such as $CuCl_2$ and $FeCl_3$, based on Cl K-edge NEXAFS analysis. Because we focused on chlorine bonded with heavy metals (zinc, copper, and iron) and the carbon matrix, inorganic chlorine (KCl) was not added to MFA for Cl K-edge

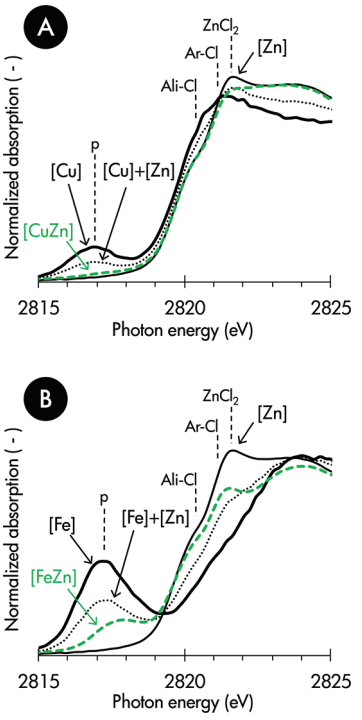

Figure 2. Cl K-edge near edge X-ray absorption fine structure (NEXAFS) after heating at 300 °C. Experimental series of (A) zinc chloride and cupric chloride and of (B) zinc chloride and ferric chloride. Spectra of [Cu]+[Zn] and [Fe]+[Zn] were calculated by a theoretical mixture ratio of each chloride. Chlorinated aromatic and aliphatic compounds were named as Ar−Cl and Ali-Cl, respectively.

NEXAFS analysis (Table S1). When zinc and cupric chloride coexisted after heating at 300 °C (MFA-[CuZn], Figure 2A), the pre-edge of $CuCl_2$ (~2817 eV, denoted as "p" of MFA-[Cu] in Figure 2A) almost vanished, there was a weak, broad shoulder at 2820−2821.2 eV due to chlorine bonded with aliphatic and aromatic compounds (Ali- and Ar−Cl),[21,24] and the spectrum shape closely resembled that of zinc chloride only (MFA-[Zn]). Calculated spectra of MFA-[Cu]+[Zn], based on a linear combination of MFA-[Cu] (0.074 mol-Cl/100 g-MFA) and MFA-[Zn] (0.073 mol-Cl/100 g-MFA) using the theoretical ratio of chlorine content, showed the pre-edge and the broad shoulder (Figure 2A). By comparing these analytical results, we drew two conclusions regarding the coexistence of zinc with copper at 300 °C: (1) chlorine bonding was maintained with zinc, but (2) dechlorination from cupric chloride was strongly promoted. These conclusions were confirmed by the similar shapes of the MFA-[CuZn] and MFA-[Zn] spectra and the lower intensity of the pre-edge of MFA-[CuZn] compared with that of MFA-[Cu]+[Zn], respectively. Additionally, a small amount of aromatic-Cls was generated in the solid phase (ref MFA-CuZn inhibition in Table 1; in fact, aromatic-Cl formation was also inhibited); the theoretical broad shoulder in MFA-[Cu]+[Zn] was observed weakly in MFA-[CuZn]. The reactivity of the carbon matrix with $CuCl_2$ was low at temperatures less than 300 °C, as reported in our previous publication.[21] These findings indicated that the temperature at which dechlorination from cupric chloride occurred was low, and chlorine entered the gas phase in the low-temperature zone (<300 °C) without reacting with carbon. The low-temperature transition of chlorine from $CuCl_2$ to the gas phase, referred to as low-Cl(g) in this study, may be an inhibition

mechanism of aromatic-Cl formation due to the coexistence of zinc.

Figure 2B shows the coexistence of zinc chloride with ferric chloride. After heating at 300 °C, the mixture of zinc and ferric chlorides (MFA-[FeZn]) exhibited a weaker pre-edge ("p" in Figure 2B) than only $FeCl_3$ (MFA-[Fe]). The postedge structure of MFA-[FeZn] at ~2819−2921 eV was similar to that of only $ZnCl_2$ (MFA-[Zn]) and differed from that of MFA-[Fe]. Additionally, the theoretical linear-combination spectrum of MFA-[Fe] (0.092 mol-Cl/100 g-MFA) and MFA-[Zn] (ditto), called MFA-[Fe]+[Zn], showed stronger pre-edge and weaker postedge structures than MFA-[FeZn]. Thus, the pre- and postedge analytical information indicated that dechlorination from ferric chloride was promoted, and chlorine was stably bonded with zinc chloride up to 300 °C due to the coexistence of zinc, respectively. Inhibition of aromatic-Cl formation was difficult to recognize by comparing the broad shoulder at 2820−2821.2 eV (Figure 2B). The strong intensity of the broad shoulder of MFA-[FeZn] (>MFA-[Fe]+[Zn]) may have been influenced by the chlorine signal of zinc chloride (MFA-[Zn]) but was not significantly influenced by chlorine bonded with the carbon matrix (Ali- and Ar−Cl) because of the low content of chlorine in aromatic-Cls detected by NEXAFS. However, we quantitatively demonstrated the inhibitory effect of MFA-FeZn using GC/MS (Table 1, Figure S1). Thus, the low-Cl(g) from $FeCl_3$ due to the coexistence of zinc may have influenced the inhibition of thermochemical aromatic-Cl formation.

To summarize this section, we showed that cupric and ferric chlorides which were known as strong promoters scattered low-Cl(g) from their structures when zinc chloride existed in the solid phase. In contrast, bulk zinc chloride was stable with increasing temperature.

Solid Surface Coated by Zinc Chloride. XPS analysis was used to determine the surface- and depth-distribution states of zinc and chloride and provided knowledge about one of the inhibition mechanisms of aromatic-Cl formation due to zinc. We measured MFA-Zn as a function of depth near the solid surface before and after heating at 300 °C (Figure 3). Zn $2p_{3/2}$ and Zn $2p_{1/2}$ peaks were clearly detected. Longer etching times resulted in weaker Zn $2p_{3/2}$ and Zn $2p_{1/2}$ intensities. The relative ratio of the atomic concentrations of Zn/Si calculated from the Zn $2p_{3/2}$ and Si $2p$ peak intensities decreased before and after heating with increasing etching time (Figure 4A). Thus, zinc was distributed and concentrated on the MFA-Zn solid surface at both room temperature and 300 °C. We also observed surface enrichment of chlorine in MFA-Zn (Figure 4B), revealing a relationship between the Cl/Si ratio and etching time. Table 2 shows that there was a positive correlation between Zn/Si and Cl/Si at both room temperature (r = 0.998) and at 300 °C (r = 0.777). The average Cl/Zn ratio during heating, calculated by dividing Cl/Si by Zn/Si, changed slightly from 1.7 to 2.2 (Table 2). Zinc was concentrated on the solid surface as $ZnCl_2$ during heating to the temperature at which aromatic-Cl formation is activated.

When cupric chloride, one of the most effective catalytic promoters, and zinc chloride coexisted in the solid phase (MFA-CuZn), zinc did not concentrate on the solid surface at room temperature, but chlorine did, as shown in Figure 4C and 4D, respectively. Zinc and chlorine had little correlation at room temperature (Table 2). When the temperature was increased to 300 °C, both zinc and chlorine showed maximal atomic concentration ratios after 60 s of etching and a positive correlation (r = 0.881). Thus, zinc and chlorine concentrated near the solid

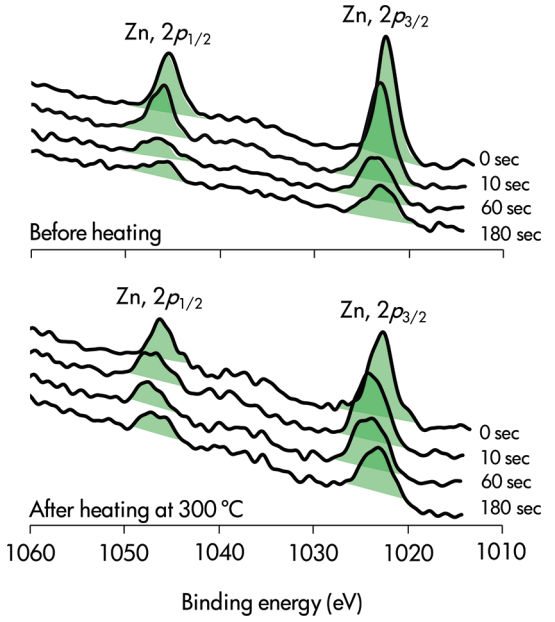

Figure 3. X-ray photoelectron spectroscopy of model fly ash (MFA) added $ZnCl_2$ (upside) before and (bottom) after heating at 300 °C.

surface with heating. Additionally, we observed a decreasing tendency in the Cl/Zn ratio, from 3.3 to 2.8 (Table 2), consistent with low-Cl(g) from $CuCl_2$, as indicated by Cl K-edge NEXAFS. Increasing concentration of near-surface zinc chloride with increasing temperature was thought to be due to the inhibition mechanism of aromatic-Cl formation promoted by cupric chloride.

Surface concentrations of zinc and chlorine (maximized with 10-s etching) before and after heating were detected when ferric and zinc chloride coexisted in the solid phase (Figure 4E, 4F; MFA-FeZn). Table 2 shows that the correlation coefficient between Zn/Si and Cl/Si increased from r = 0.433 to 0.817 with increasing temperature, suggesting that zinc and chlorine continued to concentrate on the solid surface with heating. The Cl/Zn ratio at 300 °C (= 3.3) was smaller than that at room temperature (4.2), consistent with the low-Cl(g) from $FeCl_3$ detected by Cl K-edge NEXAFS.

Increasing surface or near-surface concentrations of $ZnCl_2$ with increasing temperature were detected in MFA-Zn, -CuZn, and -FeZn. XPS analysis showed similar surface concentrations of zinc in real fly ashes (i.e., complex-mixture systems) as reported previously by Takaoka et al.[10] The effect of $ZnCl_2$ on the surface state of the solid was thought to inhibit aromatic-Cl formation by metal catalysts. At the temperature of aromatic-Cl catalysis (i.e., 300 °C), carbon gasification and formation of surface oxygen complexes (SOCs) were promoted by dynamic thermochemical changes in $CuCl_2$[21] and $FeCl_3$,[23] forming bridged structures of aromatic rings, such as PCDD/Fs and PCBs. Because of the surface concentration of $ZnCl_2$ with metal catalysts, we proposed an inhibition mechanism of decreasing reactions between the metal catalysts and the carbon matrix near the surface, inhibiting carbon gasification and blocking SOC formation. Inhibition of carbon gasification was supported by TOC data (Table 2). Figure S3 shows that the ratio of residual carbon increased by 5% and 15% with the coexistence of zinc chloride with cupric and ferric chloride, respectively. Additionally, the weak formation of bridged structures of aromatic rings, such as PCBs, confirmed that the formation of SOCs was blocked

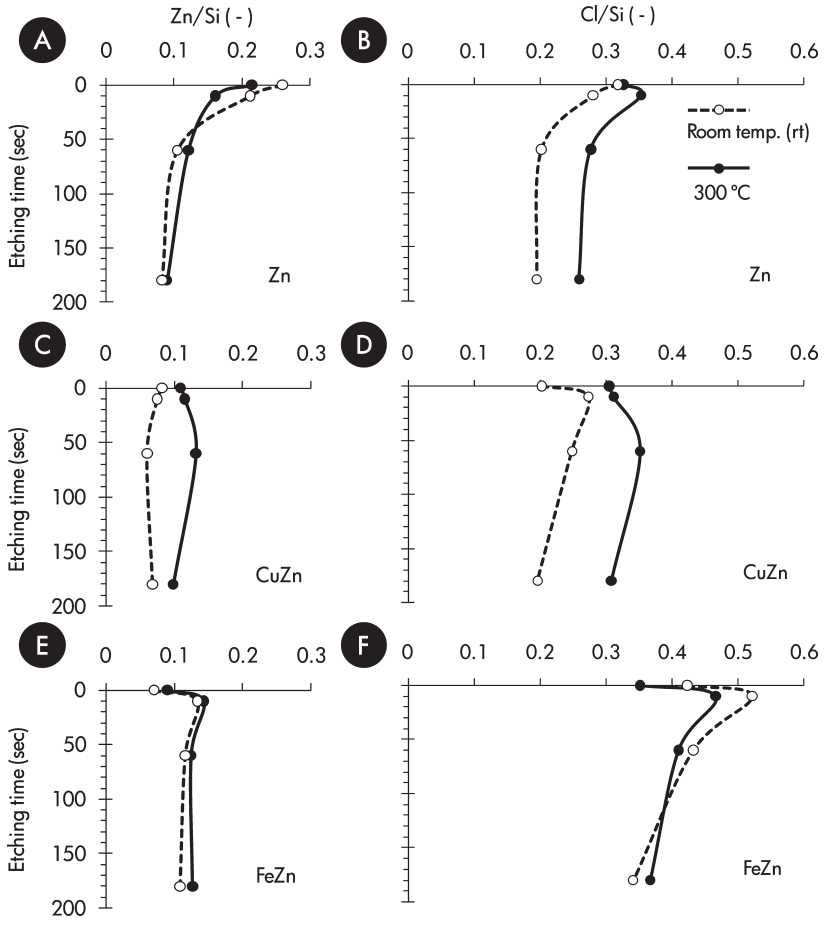

Figure 4. Zn/Si and Cl/Si ratios of model fly ash (MFA) added $ZnCl_2$ (Zn), MFA added $ZnCl_2$, and $CuCl_2$ (CuZn) MFA added $ZnCl_2$ and $FeCl_3$ (FeZn). Etching time (0, 10, 60, and 180 s) indicates information of depth at the MFA surface.

Table 2. Correlation Coefficient (r between Zn/Si and Cl/Si Ratio) and Average Cl/Zn Ratio with Standard Deviation of Model Fly Ashes (MFA) under Room Temperature (rt) and after Heating at 300 °C[a]

MFA	Temp.	r (Zn/Si vs Cl/Si)	Cl/Zn
Zn	rt	0.998	1.7 ± 0.5
CuZn	rt	−0.204	3.3 ± 0.7
FeZn	rt	0.433	4.2 ± 1.3
Zn	300 °C	0.777	2.2 ± 0.6
CuZn	300 °C	0.881	2.8 ± 0.2
FeZn	300 °C	0.817	3.3 ± 0.4

[a] Correlation coefficient r was calculated by scatter plot of Zn/Si vs Cl/Si at each temperature.

(Table 1, Figure S1). The near-surface concentration of $ZnCl_2$ might be an important factor in the inhibition mechanisms of aromatic-Cl formation by metal catalysts.

■ ASSOCIATED CONTENT

Ⓢ Supporting Information. One supporting table and three supporting figures. This material is available free of charge via the Internet at http://pubs.acs.org.

■ AUTHOR INFORMATION

Corresponding Author

*E-mail: fujimori.takashi@nies.go.jp.

■ ACKNOWLEDGMENT

We thank A. Shiono, K. Nishimura, T. Yamamoto, H. Harada, T. Tanaka, K. Oshita, and N. Takeda for their help with in situ Zn K-edge XAFS measurements; H. Tanida and T. Uruga (BL01B1) for their help with Zn K-edge XAFS measurements at SPring-8 (Proposals 2000B0309, 2001A0367, and 2004A0040); and Y. Kitajima (BL-11B) and Y. Inada (BL-9A) for their help with Cl K-edge NEXAFS measurements at the Photon Factory (Proposal 2007G069). We acknowledge financial support from the Ministry of the Environment (K1632) and a Grand-in-Aid for Young Scientists (A) from JSPS (17681008).

■ REFERENCES

(1) Kirby, C. S.; Rimstidt, J. D. Mineralogy and surface-properties of municipal solid waste ash. *Environ. Sci. Technol.* **1993**, *27*, 652–660.

(2) Eighmy, T. T.; Eusden, J. D., Jr.; Krzanowski, J. E.; Domingo, D. S.; Stampfli, D.; Martin, J. R.; Erickson, P. M. Comprehensive approach toward understanding element speciation and leaching behavior in municipal solid waste incineration electrostatic precipitator ash. *Environ. Sci. Technol.* **1995**, *29*, 629–646.

(3) Kida, A.; Noma, Y.; Imada, T. Chemical speciation and leaching properties of elements in municipal incinerator ashes. *Waste Manage.* **1996**, *16*, 527–536.

(4) Hinton, W. S.; Lane, A. M. Characteristics of municipal solid waste incinerator fly ash promoting the formation of polychlorinated dioxins. *Chemosphere* **1991**, *22*, 473–483.

(5) Chang, M.-B.; Chung, Y.-T. Dioxin contents in fly ashes of MSW incineration in Taiwan. *Chemosphere* **1998**, *36*, 1959–1968.

(6) Takaoka, M.; Yamamoto, T.; Shiono, A.; Takeda, N.; Oshita, K.; Matsumoto, T.; Tanaka, T. The effect of copper speciation on the formation of chlorinated aromatics on real municipal solid waste incinerator fly ash. *Chemosphere* **2005**, *59*, 1497–1505.

(7) Ba, T.; Zheng, M.; Zhang, B.; Liu, W.; Su, G.; Xiao, K. Estimation and characterization of PCDD/Fs and dioxin-like PCB emission from secondary zinc and lead metallurgies in China. *J. Environ. Monit.* **2009**, *11*, 867–872.

(8) Grochowalski, A.; Lassen, C.; Holtzer, M.; Sadowski, M.; Hudyma, T. Determination of PCDDs, PCDFs, PCBs and HCB emissions from the metallurgical sector in Polland. *Environ. Sci. Pollut. Res.* **2007**, *14*, 326–332.

(9) Ba, T.; Zheng, M.; Zhang, B.; Liu, W.; Su, G.; Liu, G.; Xiao, K. Estimation and congener-specific characterization of polychlorinated naphthalene emissions from secondary nonferrous metallurgical facilities in China. *Environ. Sci. Technol.* **2010**, *44*, 2441–2446.

(10) Takaoka, M.; Kuramoto, Y.; Takeda, N.; Fujiwara, T. Speciation of zinc, lead and copper on fly ash by X-ray photoelectron spectroscopy. *J. Japan Soc. Waste Manage. Experts* **2001**, *12*, 102–111(in Japanese).

(11) Shoji, T.; Huggins, F. E.; Huffman, G. P.; Linak, W. P.; Miller, C. A. XAFS spectroscopy analysis of selected elements in fine particulate matter derived from coal combustion. *Energy Fuels* **2002**, *16*, 325–329.

(12) Struis, R. P. W. J.; Ludwig, C.; Lutz, H.; Scheidegger, A. M. Speciation of zinc in municipal solid waste incineration fly ash after heat treatment: An X-ray absorption spectroscopy study. *Environ. Sci. Technol.* **2004**, *38*, 3760–3767.

(13) Gilardoni, S.; Fermo, P.; Cariati, F.; Gianelle, V.; Pitea, D.; Collina, E.; Lasagni, M. MSWI fly ash particle analysis by scanning electron microscopy-energy dispersive X-ray spectroscopy. *Environ. Sci. Technol.* **2004**, *38*, 6669–6675.

(14) Takaoka, M.; Yamamoto, T.; Tanaka, T.; Takeda, N.; Oshita, K.; Uruga, T. Direct speciation of lead, zinc and antimony in fly ash from waste treatment facilities by XAFS spectroscopy. *Phys. Scr.* **2005**, *T115*, 943–945.

(15) Oberg, T.; Bergback, B.; Filipsson, M. Catalytic effects by metal oxides on the formation and degradation of chlorinated aromatic compounds. *Chemosphere* **2008**, *71*, 1135–1143.

(16) Fujimori, T; Takaoka, M.; Takeda, N. Influence of Cu, Fe, Pb, and Zn chlorides and oxides on formation of chlorinated aromatic compounds in MSWI fly ash. *Environ. Sci. Technol.* **2009**, *43*, 8053–8059.

(17) Fujimori, T.; Takaoka, M.; Tsuruga, S.; Oshita, K.; Takeda, N. Real-time gas-phase analysis of mono- to tri-chlorobenzenes generated from heated MSWI fly ashes containing various metal compounds: Application of VUV-SPI-IT-TOFMS. *Environ. Sci. Technol.* **2010**, *44*, 5528–5533.

(18) Qian, Y.; Zheng, M.; Liu, W.; Ma, X.; Zhang, B. Influence of metal oxides on PCDD/Fs formation from pentachlorophenol. *Chemosphere* **2005**, *60*, 951–958.

(19) Hinton, W. S.; Lane, A. M. Effect of zinc, copper, and sodium on formation of polychlorinated dioxins on MSW incinerator fly ash. *Chemosphere* **1992**, *25*, 811–819.

(20) Proctor, A.; Sherwood, P. M. A. Smoothing of digital X-ray photoelectron spectra by an extended sliding least-squares approach. *Anal. Chem.* **1980**, *52*, 2315–2321.

(21) Fujimori, T.; Takaoka, M. Direct chlorination of carbon by copper chloride in a thermal process. *Environ. Sci. Technol.* **2009**, *43*, 2241–2246.

(22) Takaoka, M.; Shiono, A.; Nishimura, K.; Yamamoto, T.; Uruga, T.; Takeda, N.; Tanaka, T.; Oshita, K.; Matsumoto, T.; Harada, H. Dynamic change of copper in fly ash during de novo synthesis of dioxins. *Environ. Sci. Technol.* **2005**, *39*, 5878–5884.

(23) Fujimori, T.; Takaoka, M.; Morisawa, S. Chlorinated aromatic compounds in a thermal process promoted by oxychlorination of ferric chloride. *Environ. Sci. Technol.* **2010**, *44*, 1974–1979.

(24) Fujimori, T.; Tanino, Y.; Takaoka, M.; Morisawa, S. Chlorination mechanism of carbon during dioxin formation using Cl-K near-edge X-ray-absorption fine structure. *Anal. Sci.* **2010**, *26*, 1119–1125.

(25) Fujimori, T.; Takaoka, M.; Tanino, Y.; Oshita, K.; Morisawa, S. A metal mixture lowers the reaction temperature of copper chloride as shown using in situ quick XAFS. *J. Phys.: Conf. Ser.* **2009**, *190*, 012183.

(26) Everaert, K.; Baeyens, J. The formation and emission of dioxins in large scale thermal processes. *Chemosphere* **2002**, *46*, 439–448.

(27) Shirley, D. A. High-resolution X-ray photoemission spectrum of the valence bands of gold. *Phys. Rev. B* **1972**, *5*, 4709–4714.

(28) Addink, R.; Olie, K. Mechanisms of formation and destruction of polychlorinated dibenzo-p-dioxins and dibenzofurans in heterogeneous systems. *Environ. Sci. Technol.* **1995**, *29*, 1425–1435.

(29) Addink, R.; Olie, K. Role of oxygen in formation of polychlorinated dibenzo-p-dioxins/dibenzofurans from carbon on fly ash. *Environ. Sci. Technol.* **1995**, *29*, 1586–1590.